Site-selective Protonation of the One-electron Reduced Cofactor in [FeFe]-Hydrogenase

Konstantin Laun[a,b], Iuliia Baranova[a,c], Jifu Duan[d], Leonie Kertess[d], Florian Wittkamp[e], Ulf-Peter Apfel[e,f], Thomas Happe[d], Moritz Senger[a,g]*, Sven T. Stripp[a]*

[a] Department of Physics, Freie Universität Berlin,14195 Berlin (Germany)

[b] Department of Chemistry, Technische Universität Berlin, 10623 Berlin (Germany)

[c] Faculty of Physics, St. Petersburg State University, 198504 St. Petersburg (Russian Federation)

[d] Faculty of Biology and Biotechnology, Ruhr-Universität Bochum, 44801 Bochum (Germany)

[e] Faculty of Chemistry and Biochemistry, Ruhr-Universität Bochum, 44801 Bochum, (Germany)

[f] Fraunhofer UMSICHT, 46047 Oberhausen (Germany)

[g] Department of Chemistry, Uppsala University, 75120 Uppsala, (Sweden)

* E-mail: moritz.senger@kemi.uu.se and sven.stripp@fu-berlin.de

ABSTRACT

Hydrogenases are microbial redox enzymes that catalyze H_2 oxidation and proton reduction (H_2 evolution). While all hydrogenases show high oxidation activities, the majority of [FeFe]-hydrogenases are excellent H_2 evolution catalysts as well. Their active site cofactor comprises a [4Fe-4S] cluster covalently linked to a diiron site equipped with carbon monoxide and cyanide ligands that facilitate catalysis at low overpotential. Distinct proton transfer pathways connect the active site niche with the solvent, resulting in a non-trivial dependence of hydrogen turnover and bulk pH. To analyze the catalytic mechanism of [FeFe]-hydrogenase, we employ *in situ* infrared spectroscopy and infrared spectro-electrochemistry. Titrating the pH under H_2 oxidation or H_2 evolution conditions reveals the influence of site-selective protonation on the equilibrium of reduced cofactor states. Governed by pKa differences across the active site niche and proton transfer pathways, we find that individual electrons are stabilized either at the [4Fe-4S] cluster (alkaline pH values) or at the diiron site (acidic pH values). This observation is discussed in the context of the natural pH dependence of hydrogen turnover as catalyzed by [FeFe]-hydrogenase.

INTRODUCTION

[FeFe]-hydrogenases are gas-processing metalloenzymes that have been found in bacteria and green algae.[1–3] They serve various roles in the hydrogen metabolism of prokaryotes, including oxidation of H_2 as an energy source and proton reduction (H_2 evolution) to maintain the cellular redox equilibrium.[4] In the chloroplast of green algae, they are part of the photosynthetic electron transport chain, coupling H_2O oxidation and H_2 evolution at the reducing end of photosystem I.[5] The first crystal structures of [FeFe]-hydrogenase helped identifying accessory and catalytic iron-sulfur clusters as well as gas channels and potential proton transfer (PT) pathways.[6–12] Additionally, various biophysical techniques were employed to characterize the electronic structure of the active site cofactor, the so-called 'H-cluster' (Figure 1AB).[1] This iron-sulfur compound is formed by a [4Fe-4S] cluster connected to a bimetallic iron site *via* a bridging cysteine residue. Carbon monoxide (CO) and cyanide ligands (CN^-) tune the redox potential of the H-cluster and anchor the diiron site within the protein.[13–15] The secondary amine of the H-cluster's aminodithiolate ligand (ADT) has been suggested to serve as proton relay between the diiron site and the amino acid residues of the catalytic PT pathway.[16–21] Moreover, it acts as an inner-sphere hydrogen-bonding donor to a number of apical ligands at the distal iron ion (Fe_d).[22] Figure 1C depicts a schematic representation of the H-cluster with potential binding sites for hydrogen species.

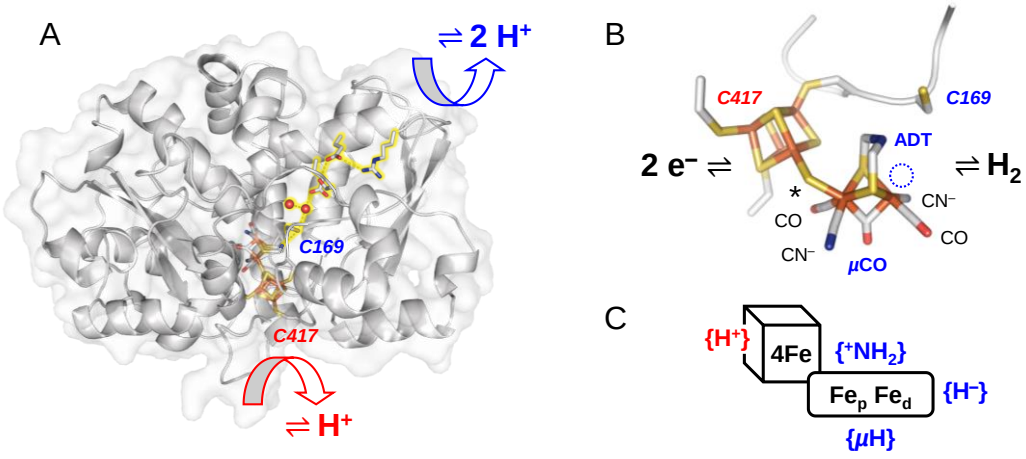

Figure 1. H-cluster and proton transfer pathways. (A) Homology model of [FeFe]-hydrogenase *Cr*HydA1. The catalytic PT pathway (including C169 close to the H-cluster) is highlighted. Cysteine C417 at the [4Fe-4S] cluster is located close to the protein surface and available for proton exchange. **(B)**

The H-cluster comprises a [4Fe-4S] cluster linked to the catalytic diiron site *via* a bridging cysteine (*). The diatomic ligands are labelled (crystal structure of **Hox** 4XDC). Most likely, the ADT ligand serves as proton relay between H-cluster (dashed circle) and C169 of the catalytic PT pathway (blue labels). At the [4Fe-4S] cluster, C417 may receive a proton directly from the solvent *via* a second PT pathway (red labels). **(C)** Schematic representation of the H-cluster highlighting potential protonation site. This includes the [4Fe-4S] cluster {H^+}, the ADT ligand {$^+NH_2$}, the apical binding site of Fe_d {H^-}, and the Fe-Fe bridging site {μH}.

The diiron site and the [4Fe-4S] cluster exist in an oxidized and reduced form each, resulting in a total of four different redox species: the oxidized state, **Hox**, the 1e$^-$-reduced states **Hred´** (reduced [4Fe-4S] cluster) and **Hred** (reduced diiron site) as well as the 'super-reduced' state, **Hsred**.[23–30] An additional 2e$^-$-reduced state, **Hhyd**, is comprised of a reduced [4Fe-4S] cluster and a formally over-oxidized diiron site with a terminal hydride ligand (H^-).[31–33] Additional states include the CO-inhibited states **Hox-CO** and **Hred´-CO** and the oxidized protonated state, **HoxH**.[27,30] While most authors agree on the importance of **Hred´** and **Hhyd** in hydrogen turnover, the protonation state, cofactor geometry, and involvement in catalysis of **Hred** and **Hsred** are under discussion.[34]

Both **Hred´** and **Hred** are enriched upon proton-coupled electron transfer (PCET). Previously, we suggested that a cysteine residue coordinating the [4Fe-4S] cluster may bind a proton in **Hred´** (Figure 1B)[29]; however, there is no consensus regarding the nature of protonation and cofactor geometry in **Hred**. Sommer *et al.* presumed protonation of the ADT ligand ($^+NH_2$) and a shift of the μCO ligand into a 'semi-bridging' position at Fe_d as seen in a crystal structure grown under H_2.[35,36] Ratzloff *et al.* proposed a $^+NH_2$ geometry with a conserved μCO ligand in **Hred**[37], which was supported in recent infrared studies by Birrell *et al.* and Lorent *et al.* that identified a μCO ligand for **Hred** and **Hsred** at cryogenic temperatures.[38,39] In contrast, our infrared evaluation of **Hred** and **Hsred** at ambient temperatures implied the formation of a bridging hydride species (μH) and an apical CO ligand at Fe_d.[28] Such changes would

exclude **Hred** and **Hsred** from the catalytic cycle as a μH geometry was calculated to be rather unreactive.[40–42] Following the time-dependent evolution of individual H-cluster bands by transient infrared spectroscopy at ambient temperature, Sanchez *et al.* proposed the kinetic competence of both **Hred´** and **Hred**.[43] Unfortunately, the spectroscopic marker bands that were used to follow **Hred** in this study are nearly identical for the μCO and the μH geometry, impeding any kinetic discrimination.[38,39] We presume that the cryogenic states may represent kinetically trapped intermediates.[44]

In this study, we investigate the pH-dependent accumulation of $1e^-$-reduced H-cluster states in the [FeFe]-hydrogenase from *Chlamydomonas reinhardtii*, *Cr*HydA1, to understand the equilibrium of **Hred´** and **Hred** under turnover conditions. Making use of *in situ* attenuated total reflection Fourier-transform infrared (ATR FTIR) spectroscopy and spectro-electrochemistry under H_2 oxidation or H_2 evolution conditions, we found consistent trends for an accumulation of **Hred´** towards alkaline pH values whereas the accumulation of **Hred** increases towards acidic pH values. This observation is explained by site-selective PCET to either the diiron site or the [4Fe-4S] cluster, guided by differences in the proton affinity. Our findings are employed to distinguish catalytic from regulatory H-cluster states and inspire a molecular understanding of the pH-dependent hydrogen turnover of [FeFe]-hydrogenase.

EXPERIMENTAL

Protein purification and activation. All experiments involving *Cr*HydA1 were performed under strictly anaerobic conditions. Native apo-protein and amino acid variants C417SDH were expressed in *Escherichia coli* host strain BL21 (DE3) ΔiscR and purified by strep-tactin affinity chromatography as described previously.[45,46] The synthetic mimics of the native ADT complex and artificial propanedithiolate complex (PDT) were synthesized following literature procedures.[17] Apo-protein was activated in the presence of ADT or PDT at a 10-fold molar excess. After an incubation period of at least 1 h at 25 °C, size-exclusion chromatography was employed to remove redundant complex.[18] Activated *Cr*HydA1 was eluted in 10 mM Tris/HCl (pH 8). For native *Cr*HydA1, sodium dithionite was avoided to

prevent accumulation of **HoxH** and **Hhyd** at low pH values.[30,32] Enzyme was concentrated to ~1 mM and stored anaerobically at −80 °C.

ATR FTIR spectroscopy. The FTIR spectrometer (Tensor27, Bruker) was equipped with a triple-reflection ZnSe/Si crystal ATR cell (Smith Detection) and placed in an anaerobic chamber. Infrared spectra were recorded with 80 kHz scanning velocity at a spectral resolution of 2 cm^{-1} (MCT detection). Under these conditions, the time-resolution of data acquisition is in the range of seconds (i.e., five interferometer scans in forward/ backward direction). ATR FTIR measurements were performed at 25°C and on hydrogenase films derived by controlled dehydration and rehydration of 1 µl protein sample as reported earlier.[27] Each sample was diluted 1:1 (~0.5 mM *Cr*HydA1) with mixed buffer containing 50 mM Tris, MES, and PIPPS to adjust the desired pH value.

The anaerobically purified and activated [FeFe]-hydrogenase typically contained the H-cluster in various states. **Hox** was enriched in the film under a constant stream of N_2 aerosol for 30 – 60 minutes. A constant gas stream (1.5 L min^{-1}) was adjusted with digital mass flow controllers (SmartTrak, Sierra). Then, H_2 was added to the N_2 stream *via* separate flow controllers and passed through a wash bottle containing 150 mL mixed buffer (0.1 – 100% at ambient pressure). The aerosol was fed into a gas-tight polychlorotrifluoroethylene (PCTFE) compartment, attached on top of the ATR crystal plate and equipped with six optional gas inlets, a manometer for pressure control, and a transparent glass window for UV/Vis irradiaton.[27] For each H_2 concentration step, the film was equilibrated for 2.5 min (Figure S1).

ATR FTIR spectro-electrochemistry. The pH-dependent reduction of *Cr*HydA1 in the absence of H_2 was analyzed by ATR FTIR spectro-electrochemistry.[28,29] For this, 1 µL protein sample (diluted with 50 mM mixed buffer pH 9 – 5) was injected into a 9 µm thin gold mesh on top of an ATR silicon crystal. The mesh was covered with 8 kDa dialysis membrane to protect the film from dilution. A custom-made PCTFE electrochemical cell was attached to the ATR crystal plate and filled with 3 mL electrolyte buffer (50 mM mixed buffer pH 9 – 5 including 500 mM KCl as electrolyte), that was purged with N_2 throughout

the whole experiment. After 60 – 90 minutes, the film was fully hydrated. The gold mesh was connected with the working electrode, platinum wire was used as counter electrode, and an Ag/AgCl electrode served as reference (+230 mV vs SHE, as determined with 1 mM methyl viologen at pH 7).[29] After complete oxidation at -100 mV vs SHE, the potential was lowered incrementally from -150 mV to -850 mV in steps of 50 mV with a fixed duration of 20 minutes for each step (Figure S2) until no further spectral changes were observed. Midpoint potentials were estimated from bi-sigmoidal fits. Although the lack spectral changes after 20 min suggested steady-state conditions, smaller changes in current hinted at imperfect equilibria, in particular at strongly reducing potential (Figure S2). Thus, we refrained from Nernst-fitting and a quantitative, comparative analysis of midpoint potentials.

Data treatment. All absorbance spectra were derived from single channel spectra of reference (ZnSe/Si) and sample (ZnSe/Si + protein) in OPUS software. Then, data was exported to a home-written routine, as described previously.[30] In the frequency regime of the H-cluster (2150 – 1750 cm^{-1}), absorbance spectra were subtracted with a polynomial function simulating the broad combination band of liquid water underneath the sharp CO/CN^- bands of the H-cluster (Figures S1A and S2A). This gave rise to baseline-corrected spectra as shown in Figures S1B and S2B. Reference spectra (Figure 2 and Figure S3) allowed determining fit parameters for all observed redox states (frequency, intensity, band width, and peak ratio, see Table S1), as described earlier.[30] The sum of peak area (2 CN^- + 3 CO) for a given redox state was obtained by simulation of spectral data with the fixed fit parameters that represent the population in relation to the population of the other redox states. This value (%) and was plotted against time illustrating how the system converges into new redox equilibria upon disturbance (i.e., changes in H_2 concentration in Figure S1C or electrochemical potential in Figure S2C). For the last step of data evaluation, the population of redox states was plotted as a function of H_2 concentration or electrochemical potential.

RESULTS

All experiments were performed with the [FeFe]-hydrogenase *Cr*HydA1 under ambient conditions. In the first step, ATR FTIR spectroscopy and spectro-electrochemistry[27–29] were employed to extract the IR signatures of all relevant redox states (Table 1 and Figure S3). Figure 2A shows how ATR FTIR spectro-electrochemistry at alkaline or acidic conditions facilitated recording difference spectra for the transition from **Hox** into **Hred´** (top, pH 9, -650 *minus* -450 mV vs SHE) and **Hred** into **Hsred** (bottom, pH 5, -750 *minus* -550 mV vs SHE). The overall downshift of the cofactor bands from **Hox** → **Hred´** and **Hred** → **Hsred** has been attributed to a reduction of the [4Fe-4S] cluster (Figure 2B).[25,26] Opposed to the **Hox** → **Hred´** difference spectrum, the **Hred** → **Hsred** difference spectrum shows no signal around 1800 cm^{-1} (yellow mark-up, dashed line). This highlights the lack of a μCO ligand at the reduced diiron site (Figure 2B). Moreover, note the absence of other H-cluster species, which confirms the assignment of bands at 1961 cm^{-1} and 1953 cm^{-1} to **Hred** and **Hsred**, respectively (blue mark-up). The small band at 1972 cm^{-1} is unrelated to any known redox state. It has been assigned to **Hhyd:red** under cryogenic conditions[39]; however, the spectrum lacks the respective μCO band at 1851 cm^{-1}. Therefore, **Hred** and **Hsred** are depicted with a terminal CO ligand and a μH ligand instead of a μCO ligand in Figure 2B.[28]

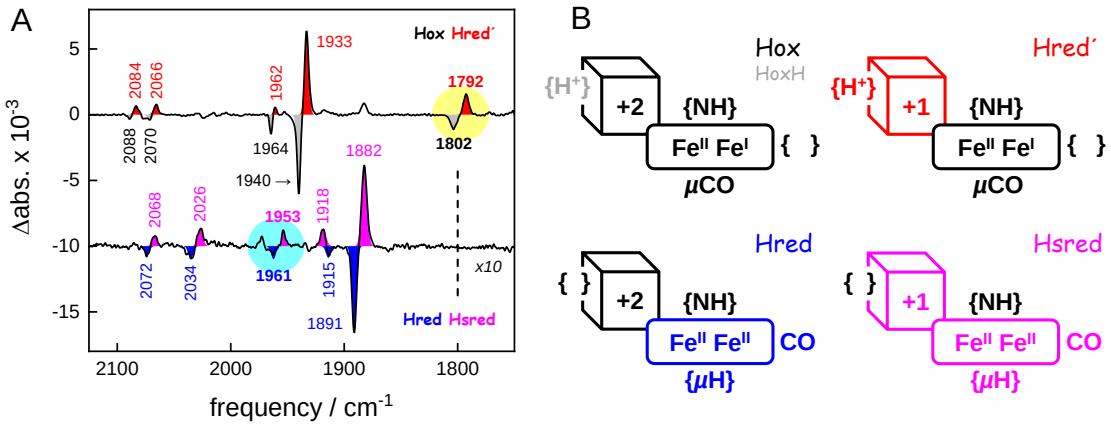

Figure 2. Characterization of key H-cluster states. (A) FTIR spectro-electrochemistry difference spectra for the transitions **Hox** → **Hred´** (top spectrum, pH 9, -650 *minus* -450 mV vs SHE) and **Hred** → **Hsred** (bottom spectrum, pH 5, -750 *minus* -550 mV vs SHE). The overall downshift has been attributed to redox changes at the [4Fe-4S] cluster. In contrast to the **Hox** → **Hred´** difference spectrum

(yellow mark-up), no μCO band is observed for **Hred** and **Hsred** (dashed line). Instead terminal CO bands appear at 1961 cm^{-1} and 1953 cm^{-1} for **Hred** and **Hsred** (yellow mark-up). **(B)** Proposed H-cluster geometries. The rectangle represents the diiron site including ADT ligand (NH), Fe-Fe bridging ligand (μCO, μH), and the apical binding site of Fe_d (vacant or occupied with CO). The cube represents the [4Fe-4S] cluster. Colors hint at differences relative to **Hox**.

Table 1. Vibrational and electronic properties of different H-cluster states. * In **Hox-CO**, vibrational coupling results in an additional IR band at 2012 cm^{-1}. ** The low-frequency μCO ligand moved into a terminal position in **Hred** and **Hsred**.

	CN^- / cm^{-1}		**CO / cm^{-1}**			**[4Fe-4S]**	**[FeFe]**
Hox	2088	2070	1964	1940	1802	+2	+3
Hox-CO	2092	2082	1968	1962*	1812	+2	+3
Hred´	2084	2066	1962	1933	1793	+1	+3
Hhyd	2082	2068	1978	1960	1860	+1	+2
Hred	2072	2034	1961**	1915	1891	+2	+2
Hsred	2068	2026	1953**	1918	1882	+1	+2

To address the pH-dependent population of H-cluster states under H_2 oxidation conditions, we investigated *Cr*HydA1 by ATR FTIR spectroscopy at different H_2 concentration without external potential control. Direct proof for the hydrogenase-catalyzed cleavage of H_2 came from D_2 oxidation experiment in aqueous environment.[32] Moreover, H_2 oxidation induces an accumulation of reduced H-cluster states so that we were able to follow the increase and decrease of redox state populations as a function of atmospheric H_2 and time. As an example, Figure 3A depicts a series of baseline-corrected ATR FTIR absorbance spectra in the CO regime of the H-cluster recorded after 2.5 min under 0 – 100% H_2 (steady-state conditions, compare Figure S1). We note that residual, unidentified H-cluster states were

present in the spectra. As these contribution did not to interfere with the global fit analysis (i.e., $\chi^2 < 10^{-4}$) we did consider them any further. Figure 3B illustrates how increasing the H_2 concentration from 0 – 0.1% resulted in an accumulation of 1e⁻-reduced states **Hred´** and **Hred**, which remained fairly stable between 0.1 – 3% H_2. At higher concentrations of H_2, the 2e⁻-reduced **Hsred** state dominated the spectrum. Only minor traces of the 2e⁻-reduced **Hhyd** state were observed, most likely due to the lack of sodium dithionite in the sample (see Experimental section).[32]

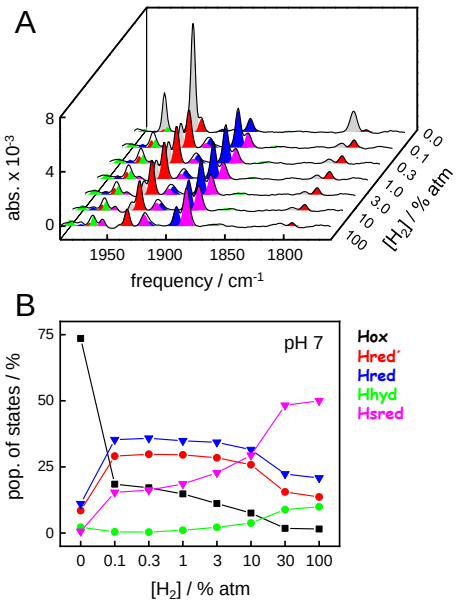

Figure 3. Composition of H-cluster states under H_2 oxidation conditions (pH 7). All data recorded on a hydrated film of *Cr*HydA1 at room temperature and 0 – 100% H_2 in the gas phase. **(A)** Series of baseline-corrected FTIR absorbance spectra in the CO regime of the H-cluster obtained after 2.5 min at each step. **(B)** State populations as a function of H_2 concentration. Between 0.1 – 3% H_2, the population of **Hred´** and **Hred** was relatively stable whereas **Hsred** dominated for H_2 > 10%.

Analogous to the experiment shown in Figure 3, six individual *Cr*HydA1 protein films between pH 10 – 5 were analyzed (Figure 4). Largely independent of pH, the oxidized state **Hox** was the most prominent species in the absence of H_2 while **Hsred** dominated the spectrum for H_2 > 10% (Figure S4). The steady-state population of **Hred´** and **Hred** is plotted as a function of H_2 and at different pH values in Figure 4AB. Here, we observed diverging trends for the accumulation of the 1e⁻-reduced states as highlighted

by the arrows: **Hred** dominated at acidic conditions whereas **Hred´** was promoted under alkaline values. Figure 4C depicts the accumulation of **Hred´** and **Hred** at 3% H_2 as a function of pH, which clearly illustrates this trend. At low pH and H_2 > 10%, an increasing accumulation of **Hhyd** was observed, which may explain the mild suppression of **Hsred** that was otherwise expected to follow the same pH dependence as **Hred** (Figure S4). Upon removal of H_2 from the gas stream, the $2e^-$-reduced states **Hhyd** and **Hsred** converted transiently into the $1e^-$-reduced states **Hred´** and **Hred**, indicating intermolecular electron transfer in the dense films[30], before the equilibrium shifted back towards **Hox** upon auto-oxidation.[22] The diverging pH dependence for the steady-state accumulation of **Hred´** and **Hred** in the presence of H_2 was found to be well conserved in this transient increase, emphasizing the robustness of all trends observed for of the $1e^-$-reduced states (Figure S5).

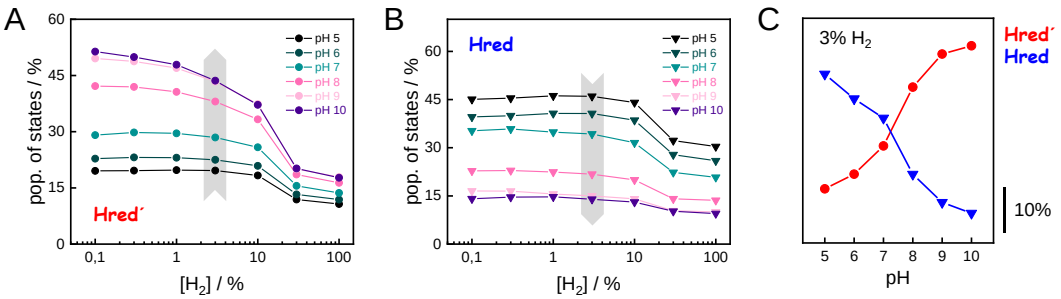

Figure 4. Accumulation of Hred´ and Hred as a function of H_2 and pH. Population of **Hred´** (panel A) and **Hred** (panel B) for six different pH values (pH 5 – 10) at 0.1 – 100% H_2. The arrows at 3% H_2 hint at an opposite pH dependence, which is clearly illustrated plotting the population of **Hred´** and **Hred** at 3% H_2 against pH (panel C).

The simultaneous presence of **Hred´** and **Hred** complicates unique conclusions regarding the mechanism of H-cluster protonation. Therefore, additional experiments were performed. First, we probed the pH dependence of H_2 oxidation with *Cr*HydA1^{PDT}. This cofactor variant lacks the secondary amine of the natural ADT ligand (Figure 1B) and allows analyzing the reduction of the [4Fe-4S] cluster (i.e., the **Hox/Hred´** transition) independent of redox chemistry at the diiron site.[26,29] Figure S6 shows that the H_2 oxidation activity of *Cr*HydA1^{PDT} increases between pH 10 – 8. While this cannot be explained by the

stoichiometry of the catalyzed reaction, the results are in agreement with earlier experiments under H_2 evolution conditions and support PCET chemistry at the [4Fe-4S] cluster.[29]

The influence of cysteinyl ligand C417 on the catalytic properties of *Cr*HydA1 has been addressed by site-directed mutagenesis earlier.[46,47] Here, we analyzed three cysteine variants to compare the composition of H-cluster states under H_2 oxidation conditions (Figure S7). *(i)* C417S behaved much like wild-type *Cr*HydA1 but showed a reduced percentage of **Hred´** under H_2. *(ii)* Due to electron withdrawal from the [4Fe-4S] cluster by the imidazole ligand, C417H was reported with a less negative redox potential than wild-type *Cr*HydA1.[47] In agreement with earlier observations, C417H adopted **Hred´** as a resting state and even after 12 – 18 h under N_2 we did not observe accumulation of **Hox**, reflecting the lack of H_2 evolution activity of *Cr*HydA1 C417H.[47] In the presence of H_2, the variant converted into **Hsred** (at pH 8) or **Hhyd** (pH 4) with no detectable traces of **Hred**. In the absence of H_2, low pH conditions resulted in an accumulation of **Hred´H**. *(iii)* The spectral behavior of C417D was surprisingly similar to C417H, indicative of electron withdrawal, e.g., due to hydrogen-bonding between the aspartic acid side chain and the [4Fe-4S] cluster. In variance to the histidine variant, C417D converted into **Hox** (pH 8) or **HoxH** (pH 4) after 12 – 18 h, reflecting the low but significant H_2 evolution activity of *Cr*HydA1 C417D.[46]

Overall, our data demonstrate how the equilibrium of redox states is affected by cluster ligation, proton concentration (pH), and the percentage of H_2 in the gas phase. Under H_2 oxidation conditions, virtually all H-cluster species were present at every step of the experiment, impeding an individual analysis of states. Thus, we investigated the pH-dependent population of redox states in *Cr*HydA1 under H_2 evolution conditions by injecting electrons into the systems in the absence of H_2. We employed ATR FTIR spectro-electrochemistry to follow the evolution of state populations as a function of electrochemical potential. In contrast to conventional, Moss-type[48] transmission cells, the ATR FTIR spectro-electrochemistry approach allowed H_2 to be released from the protein film which precluded product oxidation. Figure 5

depicts how the oxidized states **Hox** and **Hox-CO** were lost at reductive potentials, followed by accumulation of the 1e⁻-reduced states **Hred´** and **Hred**. Upon further reduction, accumulation of **Hsred** was observed; however, in contrast to the experiments performed under H_2 oxidation conditions (Figure 3), **Hhyd** was not observed at all. The latter observation may hint at different catalytic pathways for H_2 oxidation and H_2 evolution.[21]

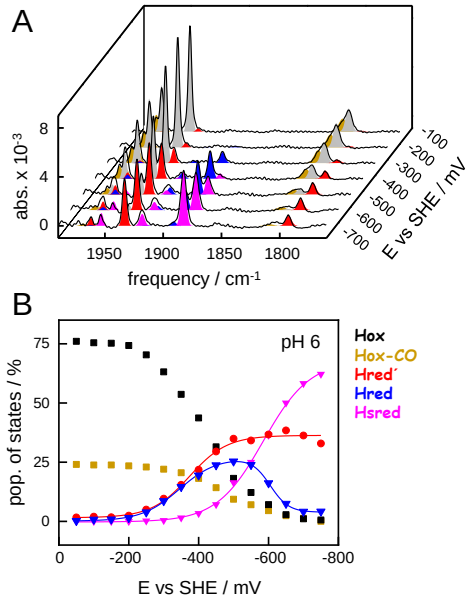

Figure 5. Composition of H-cluster states under electrochemical control (pH 6). Exemplary data recorded on a hydrated film of *Cr*HydA1 between -50 – -750 mV vs SHE and constant N_2 purging. **(A)** Series of baseline-corrected ATR FTIR absorbance spectra in the CO regime of the H-cluster obtained after 20 min at each increment of 50 mV (steady-state conditions). **(B)** State populations as a function of electrochemical potential. Sigmoidal fits allowed approximating the following midpoint potentials: **Hox/Hred´** -375 mV; **Hox/Hred** -345 mV; **Hred/Hsred** -605 mV and -585 mV vs SHE.

Analogous to the experiment shown in Figure 5, nine individual protein films were analyzed (pH 9 – 5, in steps of 0.5 pH units). Reductive currents at potentials more negative than -550 mV vs SHE (Figure S2) restricted the analysis of midpoint potentials. Instead, the maximal population of H-cluster states as a function of potential and pH value was used as the main observable. This approach allowed analyzing the 1e⁻- and 2e⁻-reduced states separately, which was not possible under H_2 oxidation conditions (Figure

4). The oxidized state **Hox** was the most prominent species at potentials more positive than -350 mV vs SHE, largely independent of pH. The accumulation of **Hsred** was found to be affected by pH more drastically, with a higher population at acidic pH values that reflects the lack of **Hhyd** in the experiment (Figure S8). Overall, we observed a mean midpoint potential around -650 mV vs SHE for **Hsred**, which leaves a potential window of ~300 mV to analyze the accumulation of the $1e^-$-reduced states. In Figure 6AB the steady-state population of **Hred´** and **Hred** is plotted as a function of potential and at different pH values. Similar to what has been observed under H_2 oxidizing conditions, **Hred** dominated at acidic conditions whereas **Hred´** was promoted under alkaline values. The arrows highlight these trends at reducing potentials; here, the population of states varies from 30 – 80 % (-550 mV vs SHE, **Hred´**) and 40 – 5% (-350 mV vs SHE, **Hred**) for increasing pH values. Figure 6C depicts the accumulation of **Hred´** and **Hred** as a function of pH. This trend is strictly conserved in the aforementioned potential window (Figure S8) and facilitated an estimation of apparent proton affinities for the accumulation of **Hred´** (pK_a > 8) and **Hred** (pK_a < 6).

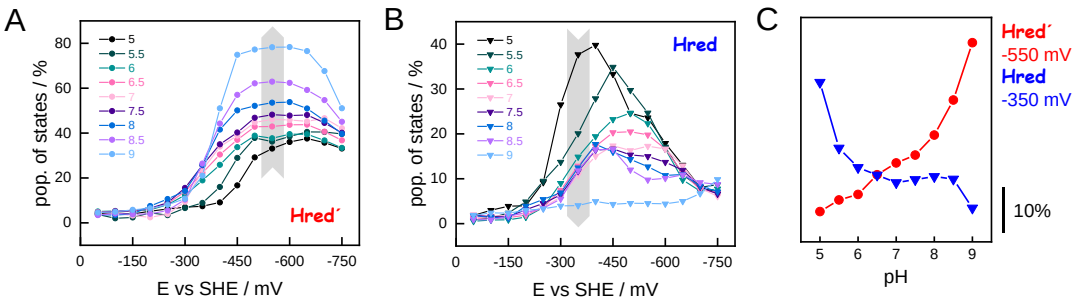

Figure 6. Accumulation of Hred´ and Hred as a function of electrochemical potential and pH. Population of **Hred´** (panel A) and **Hred** (panel B) for nine different pH values (pH 9 – 5) between -50 and -750 mV vs SHE. The arrows hint at an opposite pH dependence, which is clearly illustrated plotting the population of **Hred´** (-550 mV vs SHE) and **Hred** (-350 mV vs SHE) as function of pH (panel C).

DISCUSSION

We analyzed the [FeFe]-hydrogenase HYDA1 from *Chlamydomonas reinhardtii* by ATR FTIR spectroscopy and spectro-electrochemistry under ambient conditions. Our in-depth characterization by infrared difference spectroscopy proved the lack of cryogenic H-cluster states.[37–39] This facilitated a unique assignment of the IR pattern of **Hred** and **Hsred**, notably without a bridging CO ligand and in agreement with former reports.[23–26] Moreover, we addressed the pH-dependent accumulation of various H-cluster states. Varying the sample pH under H_2 oxidation and H_2 evolution conditions established consistent trends for the accumulation of $1e^-$-reduced H-cluster states: we observed enrichment of **Hred** under acidic conditions whereas **Hred´** prevailed at alkaline conditions. Our data on cofactor and amino acid variants highlight the importance of the [4Fe-4S] cluster for catalysis and the equilibrium of redox species.

In earlier work, we identified the pH dependence of **Hred´** formed upon reduction of the [4Fe-4S] cluster and protonation of a nearby cysteine, C417 in *Cr*HydA1.[29] Moreover, the **Hred´** state is involved in the steady-state accumulation of **HoxH**,[30] which proceeds under reducing conditions exclusively and represents the starting state for an enrichment of **Hhyd** in the presence of H_2.[32,49] While these data indicate PCET to the [4Fe-4S] cluster and emphasize the importance of redox chemistry adjacent to the diiron site, an understanding of the non-trivial pH dependence of **Hred´** and **Hred** under turnover conditions is yet to be accomplished. Due to the simultaneous presence of various reduced H-cluster states under H_2 (including **Hhyd** and **Hsred**), unraveling the PCET chemistry of **Hred´** and **Hred** was found to be challenging.[35] To this end, ATR FTIR spectro-electrochemistry facilitated analyzing the population of $1e^-$- and $2e^-$-reduced H-cluster states individually. The accumulation of **Hred** at acidic pH values and mildly reducing conditions (e.g., -350 mV vs SHE) suggests an apparent $pK_a < 6$, in agreement with the involvement of glutamic acid residues as 'bottle neck' in the catalytic PT pathway.[19] In contrast, our data for the population of **Hred´** at more reducing potentials (e.g., -550 mV vs SHE) hints at an apparent $pK_a > 8$, which reflects the greater ease of proton transfer to the [4Fe-4S] cluster *via* bulk solvent[30,34] and is in

excellent agreement with the formal pK_a of 8.1 for a cysteine sidechain. This observation is direct evidence for the pH dependence of **Hred´** in native [FeFe]-hydrogenase, in particular because the **Hred** state does not show dedicated pH dependence in this pH window. We propose to distinguish a 'high pressure', catalytic PT pathway to the diiron site from a 'low pressure', regulatory pathway to the [4Fe-4S] cluster as a common feature of [FeFe]-hydrogenases.

Both *in vivo* and *in vitro*, the pH dependence of H_2 evolution of [FeFe]-hydrogenase shows a bell-shaped distribution with a maximal activity around neutral or mildly alkaline pH values.[50–53] This has recently been confirmed by bulk electrochemistry.[54] While the increase in H_2 evolution activity between pH 9 – 7 can be attributed to rising proton concentration, our data now allows correlating the activity decrease between pH 7 – 5 to the formation of **Hred**, which clearly dominated over **Hred´** at acidic pH values. This behavior is in agreement with **Hred** and **Hsred** as 'H_2-inhibited' states[55] that bind a bridging hydride at the diiron site[28] and have been shown to play a key role in sensory [FeFe]-hydrogenases.[56–58] The ligand flip required to form a reactive terminal hydride geometry disfavors fast catalysis.[40–42] The present data support the theory that reduction and site-selective protonation at the [4Fe-4S] cluster adjusts the redox potential of the H-cluster to stabilizes a reactive geometry necessary for efficient hydrogen catalysis.[34] We suggest that similar concepts may give rise to a novel generation of biomimetic hydrogen catalysts.

ACKNOWLEDGEMENTS

We thanks all reviewers for the critical feedback. Konstantin was supported by the Einstein Foundation Berlin. The research stay of Iuliia was funded by G-RISC (P-2016b-28). We thank the Studienstiftung des Deutschen Volkes for a Kekulé Mobility Fellowship (to Leonie) and a PhD fellowship (to Florian). Ulf acknowledges funding by the DFG (under Germany´s Excellence Strategy – EXC 2033 – 390677874 – RESOLV; AP242/12-1), and the Fraunhofer Internal Programs (Grant ATTRACT 097-602175). Thomas acknowledges financial support from the Volkswagen Stiftung (Az 93412), the DFG under Germanys' Excellence Strategy – EXC-2033 (project number 390677874), and the DFG (GRK 2341

Microbial Substrate Conversion). The European Union's Horizon 2020 research and innovation programme is gratefully acknowledged for funding to Moritz (under the Marie Skłodowska-Curie grant agreement No 897555). Sven is funded by the German Research Foundation (DFG) within the framework of priority program 1927 (grant 1554/5-1).

REFERENCES

(1) Lubitz, W.; Ogata, H.; Rüdiger, O.; Reijerse, E. Hydrogenases. *Chem. Rev.* **2014**, *114* (8), 4081–4148. https://doi.org/10.1021/cr4005814.

(2) Peters, J. W.; Schut, G. J.; Boyd, E. S.; Mulder, D. W.; Shepard, E. M.; Broderick, J. B.; King, P. W.; Adams, M. W. [FeFe]- and [NiFe]-Hydrogenase Diversity, Mechanism, and Maturation. *Biochim. Biophys. Acta* **2015**, *1853* (6), 1350–1369. https://doi.org/10.1016/j.bbamcr.2014.11.021.

(3) Land, H.; Senger, M.; Berggren, G.; Stripp, S. T. Current State of [FeFe]-Hydrogenase Research - Biodiversity and Spectroscopic Investigations. *ACS Catal.* **2020**, *10*, 7069–7086. https://doi.org/10.1021/acscatal.0c01614.

(4) Greening, C.; Biswas, A.; Carere, C. R.; Jackson, C. J.; Taylor, M. C.; Stott, M. B.; Cook, G. M.; Morales, S. E. Genomic and Metagenomic Surveys of Hydrogenase Distribution Indicate H 2 Is a Widely Utilised Energy Source for Microbial Growth and Survival. *ISME J.* **2016**, *10* (3), 761–777. https://doi.org/10.1038/ismej.2015.153.

(5) Hemschemeier, A.; Happe, T. Alternative Photosynthetic Electron Transport Pathways during Anaerobiosis in the Green Alga Chlamydomonas Reinhardtii. *Biochim. Biophys. Acta - Bioenerg.* **2011**, *1807* (8), 919–926. https://doi.org/10.1016/j.bbabio.2011.02.010.

(6) Peters, J. W.; Lanzilotta, W. N.; Lemon, B. J.; Seefeldt, L. C. X-Ray Crystal Structure of the Fe-Only Hydrogenase (CpI) from Clostridium Pasteurianum to 1.8 Angstrom Resolution. *Science* **1998**, *282* (5395), 1853–1858. https://doi.org/10.1126/science.282.5395.1853.

(7) Nicolet, Y.; Piras, C.; Legrand, P.; Hatchikian, C. E.; Fontecilla-Camps, J. C. Desulfovibrio

Desulfuricans Iron Hydrogenase: The Structure Shows Unusual Coordination to an Active Site Fe Binuclear Center. *Structure* **1999**, *7* (1), 13–23. https://doi.org/10.1016/S0969-2126(99)80005-7.

(8) Cohen, J.; Kim, K.; King, P. W.; Seibert, M.; Schulten, K. Finding Gas Diffusion Pathways in Proteins: Application to O2 and H2 Transport in CpI [FeFe]-Hydrogenase and the Role of Packing Defects. *Structure* **2005**, *13* (9), 1321–1329. https://doi.org/10.1016/j.str.2005.05.013.

(9) Liebgott, P.; Leroux, F.; Burlat, B.; Dementin, S. Relating Diffusion along the Substrate Tunnel and Oxygen Sensitivity in Hydrogenase. *Nat. Chem. Biol.* **2009**, *6*, 63–70. https://doi.org/10.1038/NCHEMBIO.276.

(10) Mulder, D. W.; Shepard, E. M.; Meuser, J. E.; Joshi, N.; King, P. W.; Posewitz, M. C.; Broderick, J. B.; Peters, J. W. Insights into [FeFe]-Hydrogenase Structure, Mechanism, and Maturation. *Structure* **2011**, *19* (8), 1038–1052. https://doi.org/10.1016/j.str.2011.06.008.

(11) Lautier, T.; Ezanno, P.; Baffert, C.; Fourmond, V.; Cournac, L.; Fontecilla-Camps, J. C.; Soucaille, P.; Bertrand, P.; Meynial-Salles, I.; Léger, C. The Quest for a Functional Substrate Access Tunnel in FeFe Hydrogenase. *Faraday Discuss.* **2011**, *148*, 385. https://doi.org/10.1039/c004099c.

(12) Winkler, M.; Esselborn, J.; Happe, T. Molecular Basis of [FeFe]-Hydrogenase Function: An Insight into the Complex Interplay between Protein and Catalytic Cofactor. *Biochim. Biophys. Acta* **2013**, *1827* (8–9), 974–985. https://doi.org/10.1016/j.bbabio.2013.03.004.

(13) Knörzer, P.; Silakov, A.; Foster, C. E.; Armstrong, F. A.; Lubitz, W.; Happe, T. Importance of the Protein Framework for Catalytic Activity of [FeFe]-Hydrogenases. *J. Biol. Chem.* **2012**, *287* (2), 1489–1499. https://doi.org/10.1074/jbc.M111.305797.

(14) Siebel, J. F.; Adamska-Venkatesh, A.; Weber, K.; Rumpel, S.; Reijerse, E.; Lubitz, W. Hybrid [FeFe]-Hydrogenases with Modified Active Sites Show Remarkable Residual Enzymatic Activity. *Biochemistry* **2015**, *54* (7), 1474–1483. https://doi.org/10.1021/bi501391d.

(15) Lampret, O.; Adamska-Venkatesh, A.; Konegger, H.; Wittkamp, F.; Apfel, U.-P.; Reijerse, E. J.;

Lubitz, W.; Rüdiger, O.; Happe, T.; Winkler, M. Interplay between CN Ligands and the Secondary Coordination Sphere of the H-Cluster in [FeFe]-Hydrogenases. *J. Am. Chem. Soc.* **2017**, *139* (50), 18222–18230. https://doi.org/10.1021/jacs.7b08735.

(16) Silakov, A.; Wenk, B.; Reijerse, E.; Lubitz, W. 14N HYSCORE Investigation of the H-Cluster of [FeFe] Hydrogenase: Evidence for a Nitrogen in the Dithiol Bridge. *Phys. Chem. Chem. Phys.* **2009**, *11* (31), 6553–6554. https://doi.org/10.1039/b913085n.

(17) Berggren, G.; Adamska-Venkatesh, A.; Lambertz, C.; Simmons, T. R.; Esselborn, J.; Atta, M.; Gambarelli, S.; Mouesca, J.-M.; Reijerse, E. J.; Lubitz, W.; et al. Biomimetic Assembly and Activation of [FeFe]-Hydrogenases. *Nature* **2013**, *499* (7456), 66–69. https://doi.org/10.1038/nature12239.

(18) Esselborn, J.; Lambertz, C.; Adamska-Venkatesh, A.; Simmons, T.; Berggren, G.; Noth, J.; Siebel, J. F.; Hemschemeier, A.; Artero, V.; Reijerse, E.; et al. Spontaneous Activation of [FeFe]-Hydrogenases by an Inorganic [2Fe] Active Site Mimic. *Nat. Chem. Biol.* **2013**, *9*, 607–609. https://doi.org/10.1038/nchembio.1311.

(19) Duan, J.; Senger, M.; Esselborn, J.; Engelbrecht, V.; Wittkamp, F.; Apfel, U.-P.; Hofmann, E.; Stripp, S. T.; Happe, T.; Winkler, M. Crystallographic and Spectroscopic Assignment of the Proton Transfer Pathway in [FeFe]-Hydrogenases. *Nat. Commun.* **2018**, *9*, 4726. https://doi.org/10.1038/s41467-018-07140-x.

(20) Senger, M.; Eichmann, V.; Laun, K.; Duan, J.; Wittkamp, F.; Knör, G.; Apfel, U.-P.; Happe, T.; Winkler, M.; Heberle, J.; et al. How [FeFe]-Hydrogenase Facilitates Bidirectional Proton Transfer. *J. Am. Chem. Soc.* **2019**, *141* (43), 17394–17403. https://doi.org/10.1021/jacs.9b09225.

(21) Lampret, O.; Duan, J.; Hofmann, E.; Winkler, M.; Armstrong, F. A.; Happe, T. The Roles of Long-Range Proton-Coupled Electron Transfer in the Directionality and Efficiency of [FeFe]-Hydrogenases. **2020**, 1–10. https://doi.org/10.1073/pnas.2007090117.

(22) Duan, J.; Mebs, S.; Laun, K.; Wittkamp, F.; Heberle, J.; Hofmann, E.; Apfel, U.-P.; Winkler, M.; Senger, M.; Haumann, M.; et al. Geometry of the Catalytic Active Site in [FeFe]-Hydrogenase Is

Determined by Hydrogen Bonding and Proton Transfer. *ACS Catal.* **2019**, *9* (10), 9140–9149. https://doi.org/10.1021/acscatal.9b02203.

(23) De Lacey, A. L.; Stadler, C.; Cavazza, C.; Hatchikian, E. C.; Fernandez, V. M. FTIR Characterization of the Active Site of the Fe-Hydrogenase from Desulfovibrio Desulfuricans. *J. Am. Chem. Soc.* **2000**, *122* (45), 11232–11233. https://doi.org/10.1021/ja002441o.

(24) Roseboom, W.; De Lacey, A. L.; Fernandez, V. M.; Hatchikian, E. C.; Albracht, S. P. J. The Active Site of the [FeFe]-Hydrogenase from Desulfovibrio Desulfuricans. II. Redox Properties, Light Sensitivity and CO-Ligand Exchange as Observed by Infrared Spectroscopy. *J. Biol. Inorg. Chem.* **2006**, *11* (1), 102–118. https://doi.org/10.1007/s00775-005-0040-2.

(25) Adamska-Venkatesh, A.; Silakov, A.; Lambertz, C.; Rüdiger, O.; Happe, T.; Reijerse, E.; Lubitz, W. Identification and Characterization of the "Super-Reduced" State of the H-Cluster in [FeFe] Hydrogenase: A New Building Block for the Catalytic Cycle? *Angew. Chemie Int. Ed.* **2012**, *51* (46), 11458–11462. https://doi.org/10.1002/anie.201204800.

(26) Adamska-Venkatesh, A.; Krawietz, D.; Siebel, J. F.; Weber, K.; Happe, T.; Reijerse, E.; Lubitz, W. New Redox States Observed in [FeFe] Hydrogenases Reveal Redox Coupling within the H-Cluster. *J. Am. Chem. Soc.* **2014**, *136* (32), 11339–11346. https://doi.org/10.1021/ja503390c.

(27) Senger, M.; Mebs, S.; Duan, J.; Wittkamp, F.; Apfel, U.-P.; Heberle, J.; Haumann, M.; Stripp, S. T. Stepwise Isotope Editing of [FeFe]-Hydrogenases Exposes Cofactor Dynamics. *Proc. Natl. Acad. Sci. U. S. A.* **2016**, *113* (30), 8454–8459. https://doi.org/10.1073/pnas.1606178113.

(28) Mebs, S.; Senger, M.; Duan, J.; Wittkamp, F.; Apfel, U.-P.; Happe, T.; Winkler, M.; Stripp, S. T.; Haumann, M. Bridging Hydride at Reduced H-Cluster Species in [FeFe]-Hydrogenases Revealed by Infrared Spectroscopy, Isotope Editing, and Quantum Chemistry. *J. Am. Chem. Soc.* **2017**, *139* (35), 12157–12160. https://doi.org/10.1021/jacs.7b07548.

(29) Senger, M.; Laun, K.; Wittkamp, F.; Duan, J.; Haumann, M.; Happe, T.; Winkler, M.; Apfel, U.-P.; Stripp, S. T. Proton-Coupled Reduction of the Catalytic [4Fe-4S] Cluster in [FeFe]-Hydrogenases. *Angew. Chemie Int. Ed.* **2017**, *56* (52), 16503–16506.

https://doi.org/10.1002/anie.201709910.

(30) Senger, M.; Mebs, S.; Duan, J.; Shulenina, O.; Laun, K.; Kertess, L.; Wittkamp, F.; Apfel, U.-P.; Happe, T.; Winkler, M.; et al. Protonation/Reduction Dynamics at the [4Fe–4S] Cluster of the Hydrogen-Forming Cofactor in [FeFe]-Hydrogenases. *Phys. Chem. Chem. Phys.* **2018**, *20* (5), 3128–3140. https://doi.org/10.1039/C7CP04757F.

(31) Mulder, D. W.; Guo, Y.; Ratzloff, M. W.; King, P. W. Identification of a Catalytic Iron-Hydride at the H-Cluster of [FeFe]-Hydrogenase. *J. Am. Chem. Soc.* **2016**, *139* (1), 83–86. https://doi.org/10.1021/jacs.6b11409.

(32) Winkler, M.; Senger, M.; Duan, J.; Esselborn, J.; Wittkamp, F.; Hofmann, E.; Apfel, U.-P.; Stripp, S. T.; Happe, T. Accumulating the Hydride State in the Catalytic Cycle of [FeFe]-Hydrogenases. *Nat. Commun.* **2017**, *8* (16115), 1–7. https://doi.org/10.1038/ncomms16115.

(33) Reijerse, E. J.; Pham, C. C.; Pelmenschikov, V.; Gilbert-wilson, R.; Adamska-Venkatesh, A.; Siebel, J. F.; Gee, L. B.; Yoda, Y.; Tamasaku, K.; Lubitz, W.; et al. Direct Observation of an Iron-Bound Terminal Hydride in [FeFe]- Hydrogenase by Nuclear Resonance Vibrational Spectroscopy. *J. Am. Chem. Soc.* **2017**, *139* (12), 4306–4309. https://doi.org/10.1021/jacs.7b00686.

(34) Haumann, M.; Stripp, S. T. The Molecular Proceedings of Biological Hydrogen Turnover. *Acc. Chem. Res.* **2018**, *51* (8), 1755–1763. https://doi.org/10.1021/acs.accounts.8b00109.

(35) Sommer, C.; Adamska-Venkatesh, A.; Pawlak, K.; Birrell, J. A.; Rüdiger, O.; Reijerse, E. J.; Lubitz, W. Proton Coupled Electronic Rearrangement within the H-Cluster as an Essential Step in the Catalytic Cycle of [FeFe] Hydrogenases. *J. Am. Chem. Soc.* **2017**, *139* (4), 1440−1443. https://doi.org/10.1021/jacs.6b12636.

(36) Nicolet, Y.; De Lacey, A. L.; Vernède, X.; Fernandez, V. M.; Hatchikian, E. C.; Fontecilla-Camps, J. C. Crystallographic and FTIR Spectroscopic Evidence of Changes in Fe Coordination upon Reduction of the Active Site of the Fe-Only Hydrogenase from Desulfovibrio Desulfuricans. *J. Am. Chem. Soc.* **2001**, *123* (8), 1596–1601. https://doi.org/10.1021/ja0020963.

(37) Ratzloff, M. W.; Artz, J. H.; Mulder, D. W.; Collins, R. T.; Furtak, T. E.; King, P. W. CO-Bridged H-Cluster Intermediates in the Catalytic Mechanism of [FeFe]-Hydrogenase CaI. *J. Am. Chem. Soc.* **2018**, *140* (24), 7623–7628. https://doi.org/10.1021/jacs.8b03072.

(38) Birrell, J. A.; Pelmenschikov, V.; Mishra, N.; Wang, H.; Yoda, Y.; Rauchfuss, T. B.; Cramer, S. P.; Lubitz, W.; Debeer, S. Spectroscopic and Computational Evidence That [FeFe] Hydrogenases Operate Exclusively with CO-Bridged Intermediates. *J. Am. Chem. Soc.* **2020**, *142* (1), 222–232. https://doi.org/10.1021/jacs.9b09745.

(39) Lorent, C.; Katz, S.; Duan, J.; Julia Kulka, C.; Caserta, G.; Teutloff, C.; Yadav, S.; Apfel, U.-P.; Winkler, M.; Happe, T.; et al. Shedding Light on Proton and Electron Dynamics in [FeFe] Hydrogenases. *J. Am. Chem. Soc.* **2020**, *142* (12), 5493–5497. https://doi.org/10.1021/jacs.9b13075.

(40) Filippi, G.; Arrigoni, F.; Bertini, L.; De Gioia, L.; Zampella, G. DFT Dissection of the Reduction Step in H2 Catalytic Production by [FeFe]-Hydrogenase-Inspired Models: Can the Bridging Hydride Become More Reactive Than the Terminal Isomer? *Inorg. Chem.* **2015**, *54* (19), 9529–9542. https://doi.org/10.1021/acs.inorgchem.5b01495.

(41) Greco, C.; Bruschi, M.; Gioia, L. De; Ryde, U. A QM / MM Investigation of the Activation and Catalytic Mechanism of Fe-Only Hydrogenases. *Inorg. Chem.* **2007**, *46* (15), 5911–5921. https://doi.org/10.1021/ic062320a.

(42) Bruschi, M.; Fantucci, P.; De Gioia, L. Density Functional Theory Investigation of the Active Site of Fe-Hydrogenases. Systematic Study of the Effects of Redox State and Ligands Hardness on Structural and Electronic Properties of Complexes Related to the [2Fe](H) Subcluster. *Inorg. Chem.* **2004**, *43* (12), 3733–3741. https://doi.org/10.1021/ic035326y.

(43) Sanchez, M. L. K.; Sommer, C.; Reijerse, E.; Birrell, J. A.; Lubitz, W.; Dyer, R. B. Investigating the Kinetic Competency of CrHydA1 [FeFe] Hydrogenase Intermediate States via Time-Resolved Infrared Spectroscopy. *J. Am. Chem. Soc.* **2019**, *141* (40), 16064–16070. https://doi.org/10.1021/jacs.9b08348.

(44) Tai, H.; Hirota, S.; Stripp, S. T. Proton Transfer Mechanisms in Bimetallic Hydrogenases. *Preprints* **2020**. https://doi.org/10.20944/preprints202007.0034.v1.

(45) Kuchenreuther, J. M.; George, S. J.; Grady-Smith, C. S.; Cramer, S. P.; Swartz, J. R. Cell-Free H-Cluster Synthesis and [FeFe] Hydrogenase Activation: All Five CO and CN^- Ligands Derive from Tyrosine. *PLoS One* **2011**, *6* (5), e20346. https://doi.org/10.1371/journal.pone.0020346.

(46) Kertess, L.; Adamska-Venkatesh, A.; Rodríguez-Maciá, P.; Rüdiger, O.; Lubitz, W.; Happe, T. Influence of the [4Fe-4S] Cluster Coordinating Cysteines on Active Site Maturation and Catalytic Properties of C. Reinhardtii [FeFe]-Hydrogenase. *Chem. Sci.* **2017**, *8* (12), 8127–8137. https://doi.org/10.1039/c7sc03444j.

(47) Rodríguez-Maciá, P.; Kertess, L.; Burnik, J.; Birrell, J. A.; Hofmann, E.; Lubitz, W.; Happe, T.; Rüdiger, O. His-Ligation to the [4Fe-4S] Subcluster Tunes the Catalytic Bias of [FeFe] Hydrogenase. *J. Am. Chem. Soc.* **2019**, *141* (1), 472–481. https://doi.org/10.1021/jacs.8b11149.

(48) Moss, D.; Nabedryk, E.; Breton, J.; Mäntele, W. Redox-Linked Conformational Changes in Proteins Detected by a Combination of Infrared Spectroscopy and Protein Electrochemistry. Evaluation of the Technique with Cytochrome C. *Eur. J. Biochem.* **1990**, *187* (3), 565–572.

(49) Mészáros, L.; Ceccaldi, P.; Lorenzi, M.; Redman, H. J.; Pfitzner, E.; Heberle, J.; Senger, M.; Stripp, S. T.; Berggren, G. Spectroscopic Investigations under Whole Cell Conditions Provide New Insight into the Metal Hydride Chemistry of [FeFe]-Hydrogenase. *Chem. Sci.* **2020**, *11* (18), 4608–4617. https://doi.org/10.1039/d0sc00512f.

(50) Healey, F. P. The Mechanism of Hydrogen Evolution by Chlamydomonas Moewusii . *Plant Physiol.* **1970**, *45* (2), 153–159. https://doi.org/10.1104/pp.45.2.153.

(51) Klein, U.; Betz, A. Induced Protein Synthesis during the Adaptation to H2 Production in Chlamydomonas Moewusii. *Physiol. Plant.* **1978**, *42* (1), 1–4. https://doi.org/10.1111/j.1399-3054.1978.tb01529.x.

(52) Roessler, P.; Lien, S. Anionic Modulation of the Catalytic Activity of Hydrogenase from Chlamydomonas Reinhardtii. *Arch. Biochem. Biophys.* **1982**, *213* (1), 37–44.

https://doi.org/10.1016/0003-9861(82)90436-2.

(53) Happe, T.; Naber, J. D. Isolation, Characterization and N-terminal Amino Acid Sequence of Hydrogenase from the Green Alga Chlamydomonas Reinhardtii. *Eur. J. Biochem.* **1993**, *214* (2), 475–481. https://doi.org/10.1111/j.1432-1033.1993.tb17944.x.

(54) Ruth, J. C.; Milton, R. D.; Gu, W.; Spormann, A. M. Enhanced Electrosynthetic Hydrogen Evolution by Hydrogenases Embedded in a Redox-Active Hydrogel. *Chem. – A Eur. J.* **2020**, *26* (32), 7323–7329. https://doi.org/10.1002/chem.202000750.

(55) Fourmond, V.; Baffert, C.; Sybirna, K.; Dementin, S.; Abou-Hamdan, A.; Meynial-Salles, I.; Soucaille, P.; Bottin, H.; Léger, C. The Mechanism of Inhibition by H2 of H2-Evolution by Hydrogenases. *Chem. Commun. (Camb).* **2013**, *49* (61), 6840–6842. https://doi.org/10.1039/c3cc43297a.

(56) Chongdar, N.; Birrell, J. A.; Pawlak, K.; Sommer, C.; Reijerse, E. J.; Rüdiger, O.; Lubitz, W.; Ogata, H. Unique Spectroscopic Properties of the H-Cluster in a Putative Sensory [FeFe] Hydrogenase. *J. Am. Chem. Soc.* **2018**, *140* (3), 1057−1068. https://doi.org/10.1021/jacs.7b11287.

(57) Land, H.; Ceccaldi, P.; Mészáros, L. S.; Lorenzi, M.; Redman, H. J.; Senger, M.; Stripp, S. T.; Berggren, G. Discovery of Novel [FeFe]-Hydrogenases for Biocatalytic H2-Production. *Chem. Sci.* **2019**, *10* (43), 9941–9948. https://doi.org/10.1039/c9sc03717a.

(58) Chongdar, N.; Pawlak, K.; Rüdiger, O.; Reijerse, E. J.; Rodríguez-Maciá, P.; Lubitz, W.; Birrell, J. A.; Ogata, H. Spectroscopic and Biochemical Insight into an Electron-Bifurcating [FeFe] Hydrogenase. *J. Biol. Inorg. Chem.* **2020**, *25*, 135–149. https://doi.org/10.1007/s00775-019-01747-1.